SPANDIDOS PUBLICATIONS

ONCOLOGY LETTERS 27: 151, 2024

CFLAR: A novel diagnostic and prognostic biomarker in soft tissue sarcoma, which positively modulates the immune response in the tumor microenvironment

XU LIU, XIAOYANG LI and SHENGJI YU

Department of Orthopedics, National Cancer Center/National Clinical Research Center for Cancer/Cancer Hospital, Chinese Academy of Medical Sciences and Peking Union Medical College, Beijing 100021, P.R. China

Received September 5, 2023; Accepted January 17, 2024

DOI: 10.3892/ol.2024.14284

Abstract. Anoikis is highly associated with tumor cell apoptosis and tumor prognosis; however, the specific role of anoikis-related genes (ARGs) in soft tissue sarcoma (STS) remains to be fully elucidated. The present study aimed to use a variety of bioinformatics methods to determine differentially expressed anoikis-related genes in STS and healthy tissues. Subsequently, three machine learning algorithms, Least Absolute Shrinkage and Selection Operator, Support Vector Machine and Random Forest, were used to screen genes with the highest importance score. The results of the bioinformatics analyses demonstrated that CASP8 and FADD-like apoptosis regulator (CFLAR) exhibited the highest importance score. Subsequently, the diagnostic and prognostic value of CFLAR in STS development was determined using multiple public and in-house cohorts. The results of the present study demonstrated that CFLAR may be considered a diagnostic and prognostic marker of STS, which acts as an independent prognostic factor of STS development. The present study also aimed to explore the potential role of CFLAR in the STS tumor microenvironment, and the results demonstrated that CFLAR significantly enhanced the immune response of STS, and exerted a positive effect on the infiltration of $CD8^+$ T cells and M1 macrophages in the STS immune microenvironment. Notably, the aforementioned results were verified using multiplex immunofluorescence analysis. Collectively, the results of the present study demonstrated that CFLAR may act as a novel diagnostic and prognostic marker for STS, and may positively regulate the immune response of STS. Thus, the present study provided a novel theoretical basis for the use of CFLAR in STS diagnosis, in predicting clinical outcomes and in tailoring individualized treatment options.

Correspondence to: Professor Shengji Yu, Department of Orthopedics, National Cancer Center/National Clinical Research Center for Cancer/Cancer Hospital, Chinese Academy of Medical Sciences and Peking Union Medical College, 17 South Lane, Panjiayuan, Chaoyang, Beijing 100021, P.R. China
E-mail: zlyygk@163.com

Abbreviations: STS, soft tissue sarcoma; CFLAR, CASP8 and FADD-like apoptosis regulator; ARGs, anoikis-related genes; ECM, extracellular matrix; LASSO, Least Absolute Shrinkage and Selection Operator; SVM, Support Vector Machine; RF, Random Forest; TME, tumor microenvironment; TCGA, The Cancer Genome Atlas; GTEx, Genotype-Tissue Expression; GEO, Gene Expression Omnibus; ROC, receiver operating characteristic; AUC, area under the curve; GO, Gene Ontology; PPI, protein-protein interaction; UMAP, uniform manifold approximation and projection; RT-qPCR, reverse transcription-quantitative PCR; mIF, multiplex immunofluorescence; DEARGs, differentially expressed ARGs; OS, overall survival; ICIs, immune checkpoint inhibitors; TCR, T-cell receptor; MAPK, mitogen-activated protein kinase; ERK, extracellular-regulated protein kinase; RIP1, receptor-interacting protein 1; MEK1, MAPK/ERK kinase 1; MEK2, MAPK/ERK kinase 2; TRAF, tumor necrosis factor receptor-associated factor

Key words: anoikis, machine learning, CFLAR, STS, TME

Introduction

Soft tissue sarcoma (STS) constitutes a rare group of heterogenous tumors, accounting for ~1% of all adult malignancies globally (1). STS often originates from mesenchymal tissues and displays multifarious clinical behaviors (2). In a previous study, elderly patients with STS exhibited a 5-year relative survival rate of <50%, indicating a high risk of death (3). At present, surgery remains the first option for STS treatment (4); however, STS is often diagnosed following pathological assessment of tissues in resection surgery, and late diagnosis may impact STS treatment. In addition, STS exhibits a high susceptibility to distant metastasis and recurrence. The results of a previous study demonstrated that ~50% of patients with localized STS experienced distant metastasis, predominantly affecting the lungs, which resulted in a poor prognosis (5). Thus, the identification of novel therapeutic targets, as well as dependable diagnostic and prognostic factors, is crucial to achieve effective and personalized treatment.

The extracellular matrix (ECM) serves as a crucial anchor for healthy epithelial cells, while also providing essential signals for maintaining cell integrity, including the promotion of proliferation, differentiation and apoptosis. Following detachment from the ECM, cells undergo anoikis, a type of

caspase-mediated apoptosis. Cells may exhibit a broad range of responses to a loss of adhesion, and these include diverse signaling and apoptotic pathways, such as the MAPK/ERK, PI3K/Akt and JNK signaling pathways, the death receptor pathways and the mitochondrial pathways (6,7). Following detachment from the cancer primary lesion, malignant cells undergo anoikis and are eliminated; however, a small subset of cells may evade anoikis through reprogramming intrinsic signals, enabling them to survive the invasion, recycling and extravasation stages, which are collectively referred to as anchorage-independent growth. This process ultimately leads to the formation of distant metastases (8). The development of anoikis resistance in aggressive tumor cells is recognized as a key factor contributing to tumor progression (9-11). The results of a previous study on osteosarcoma demonstrated an association between anoikis-related genes (ARGs) and prognosis and the immune landscape. However, to the best of our knowledge, the specific association between anoikis and STS has yet to be fully understood.

In mammalian cells, CASP8 and FADD-like apoptosis regulator (CFLAR), also known as c-Flip, is an important regulatory protein in the extrinsic apoptotic pathway (12). Several transcript variants encoding different isoforms have previously been reported. The short form, CFLAR, contains two N-terminal death effector domains, whereas the long form, CFLARL, contains an additional pseudo-caspase domain, in which the active center cysteine residue that confers the proteolytic activity of caspases is substituted by a tyrosine residue (13). CFLAR serves a critical role in fundamental intracellular processes, such as inflammation and apoptosis (14,15). CFLAR has also been regarded as a potential therapeutic target in various types of cancer (16). The results of a previous study detected elevated protein expression levels of CFLAR in lung metastatic osteosarcoma compared with those in primary tumors (17). However, the protein expression profile and mechanism of action of CFLAR in STS are poorly understood, and further investigations are required.

The present study employed three machine learning algorithms, namely, Least Absolute Shrinkage and Selection Operator (LASSO), Support Vector Machine (SVM) and Random Forest (RF), to identify CFLAR from genes associated with STS (ARGs). The aim of the study was to explore the diagnostic and prognostic value of CFLAR in STS and to investigate the effects of CFLAR on the STS tumor microenvironment (TME). Through these approaches, we seek to deepen our understanding of the role of CFLAR in the progression of STS and to provide new insights into the diagnosis and treatment of STS.

Materials and methods

Raw data. The Cancer Genome Atlas (TCGA)-SARC RNA sequencing (RNA-seq) data from 265 cases of STS (healthy samples, 2 cases; tumor samples, 263 cases), corresponding data on the clinical characteristics of 256 cases (those with complete data) from TCGA, and RNA-seq data from 911 healthy cases (healthy muscle and adipose tissue) from the Genotype-Tissue Expression (GTEx) database were downloaded from UCSC Xena database (https://xenabrowser.net/datapages/). Notably, the two aforementioned datasets were merged into one dataset for subsequent experiments, referred to as GTEx~TCGA-SARC. RNA-seq and clinical data from 24 liposarcoma cases and 16 malignant peripheral nerve sheath tumor cases in GSE17118 (18), RNA-seq data from 149 liposarcoma cases and 9 healthy cases in GSE21124 (19) and single cell RNA-Seq data of 16,872 cells from 12 human synovial sarcoma cases in GSE131309 (20) were obtained from the Gene Expression Omnibus (GEO) database (https://www.ncbi.nlm.nih.gov/geo/).

Differential expression analysis and acquisition of ARGs. GTEx~TCGA-SARC was used for the differential analysis of STS and healthy tissue samples. The analysis was conducted using the 'limma' R Package (https://bioconductor.org/packages/release/bioc/html/limma.html) (21) following normalization, and a filter was applied to obtain significantly differentially expressed genes (|log fold change|>1 and adjusted P<0.05). In addition, a list of ARGs was obtained from GeneCards (https://www.genecards.org/) and Harmonizome (https://maayanlab.cloud/Harmonizome/).

Identification and validation of diagnostic markers that distinguish between healthy tissue and STS. To identify novel biomarkers for STS in the GTEx~TCGA-SARC dataset, three different machine learning algorithms, LASSO, RF and SVM, were utilized (22-24). LASSO logistic regression with low lambda was conducted using the 'glmnet' package in R statistical software (https://CRAN.R-project.org/package=glmnet) (25), and the RF analysis was performed using the 'randomForest' package (https://CRAN.R-project.org/package=randomForest) (26). The SVM classifier was created using the 'e1071' package (https://CRAN.R-project.org/package=e1071) (27). The overlapping genes of the three models were subsequently identified. The Gini coefficient method in RF was used to determine the significance index of genetic variables. To evaluate the effectiveness of the significant biomarkers, the validation set GSE21124 was utilized, and receiver operating characteristic (ROC) curve analyses were conducted. The predictive ability of the algorithm was assessed through measuring the area under the curve (AUC). P<0.05 was considered to indicate a statistically significant difference.

Cox regression analysis. In the analysis of the TCGA-SARC dataset, a total of 132 patients with complete clinical information were selected. The 'survival' package in R statistical software was employed to perform both univariate and multivariate Cox regression analyses (https://CRAN.R-project.org/package=survival) (28). Univariate Cox regression analysis was used to identify the potential association between ARGs and STS prognosis, and the multivariate Cox regression analysis was used to determine the potential independent prognostic significance of CFLAR in STS. In addition, all variables included in the multivariate Cox regression analysis met the assumption of proportional hazards.

Survival analysis and time-ROC. Survival analysis was conducted using the 'Survminer' package in R statistical software (https://CRAN.R-project.org/package=survminer) (29). The data sets used were TCGA-SARC and GSE17118.

The Kaplan-Meier (KM) method was used to generate a survival curve and the log-rank test was applied to assess the statistical significance. P<0.05 was considered to indicate a statistically significant difference. Time-ROC was conducted using the 'timeROC' package in R statistical software (https://CRAN.R-project.org/package=timeROC) (30). Notably, 1-, 3- and 5-year ROC curves were plotted, and the corresponding AUCs were calculated. Curves of AUC over time were also plotted.

Immune infiltration and function analysis. Using CIBERSORTx analysis (https://cibersortx.stanford.edu/index.php) with a 'PERM' parameter set to 1,000 and a P-value cut-off of <0.05, the level of immune cell infiltration was measured in STS samples of TCGA-SARC. The samples were stratified into high and low CFLAR expression groups based on the median CFLAR expression value in the TCGA-SARC cohort. The relative proportions of individual immune cell types were calculated within the samples. Subsequently, a boxplot of 22 immune cell abundances was generated using the 'ggpubr' package (https://CRAN.R-project.org/package=ggpubr) (31). Spearman's rank correlation coefficient was performed to determine the potential association between immune cell infiltration and CFLAR expression, and dot-line and lollipop charts were generated accordingly. Single sample gene set enrichment analysis implemented in the R statistical software package 'GSVA' was used to calculate the immune function score in the TCGA-SARC cohort (https://bioconductor.org/packages/release/bioc/html/GSVA.html) (32), and the results are displayed in a boxplot. The independent sample t-test was used to compare differences between two groups.

TME score. The 'estimate' package in R was used to calculate the 'StromalScore', 'ImmuneScore' and 'ESTIMATEScore' between STS samples with high and low CFLAR expression in TCGA-SARC dataset (https://bioconductor.org/packages/release/bioc/html/estimate.html) (33). The results are displayed in a boxplot. The independent sample t-test was used to compare differences between two groups.

Efficacy analysis of immune checkpoint inhibitors (ICIs) in STS. The correlation (Spearman's analysis) between established ICI targets and CFLAR expression was analyzed. Subsequently, a correlation heatmap was generated to determine the potential role of CFLAR in ICI efficacy in STS. The aforementioned analysis applied the TCGA-SARC data set.

Pathway and functional enrichment analysis, and protein-protein interaction (PPI) network generation. The Gene Ontology (GO) analysis utilized the enrichGO function in the R package 'clusterProfiler' (https://bioconductor.org/packages/release/bioc/html/clusterProfiler.html) (34) and incorporated genome-wide annotations provided by the Bioconductor project (https://www.bioconductor.org/) (35). Based on the GO analysis, the specific functions of CFLAR co-upregulated genes were explored. A PPI network was generated using the STRING database (https://cn.string-db.org/), based on the protein interactions between CFLAR co-upregulated genes. The aforementioned analysis applied the TCGA-SARC data set.

Single-cell quality control, dimension reduction and cell type annotation. The complete single-cell sequencing data analysis utilized the 'Seurat' package in R statistical software, applied to the dataset GSE131309 (https://CRAN.R-project.org/package=Seurat) (36). Cells expressing between 50 and 9,000 genes were identified, with a mitochondrial gene cut-off of 5% for further filtration. Following the identification of 1,500 hypervariable genes, 20 principal components were adjusted to generate cell clusters. Subsequently, uniform manifold approximation and projection (UMAP) dimensionality reduction was performed using the data, and 20 clusters were generated. CellMarker 2.0 (http://bio-bigdata.hrbmu.edu.cn/CellMarker/) was used to manually annotate the single-cell sequencing data and eight cell types were annotated (37,38). The expression distribution of CFLAR was explored in single-cell sequencing data.

Human tissue specimens and reverse transcription-quantitative (RT-q)PCR. In this study, 45 STS tumor tissues and 18 frozen surgically resected para-carcinoma tissues, all obtained from the Sample Bank of the National Cancer Center/National Clinical Research Center for Cancer/Cancer Hospital, Chinese Academy of Medical Sciences and Peking Union Medical College (Beijing, China), were analyzed. These samples represented a cohort of 45 patients, with a mean age of 42.3 years (ranging from 32 to 52 years), and a nearly balanced sex ratio of 23 males to 22 females. Total RNA was extracted from tissues using TRIzol® reagent (Invitrogen; Thermo Fisher Scientific, Inc.). Primers for CFLAR and GAPDH were diluted in ddH_2O with SYBR Green PCR Master Mix (Wuhan Servicebio Technology Co., Ltd.). The primer sequences were as follows: CFLAR forward, 5'-AGAGTGAGGCGATTTGACCTG-3' and reverse, 5'-GTCCGAAACAAGGTGAGGGTT-3'; and GAPDH forward, 5'-GGAAGCTTGTCATCAATGGAAATC-3' and reverse, 5'-TGATGACCCTTTTGGCTCCC-3'. The reverse transcription was performed using the SweScript All-in-One First-Strand cDNA Synthesis SuperMix for qPCR (One-Step gDNA Remover) from Wuhan Servicebio Technology Co., Ltd. The reverse transcription process involved the following temperature steps: 25°C for 5 min, 42°C for 30 min and 85°C for 5 sec. qPCR Thermocycling Conditions were as follows: Initial denaturation at 95°C for 30 sec, denaturation at 95°C for 15 sec and annealing/extension at 60°C for 30 sec. For the melting curve stage, the temperature was raised from 65°C to 95°C, with fluorescence collection at every 0.5°C increase. Each sample was assessed in triplicate. CFLAR mRNA expression levels were quantified using the $2^{-\Delta\Delta Cq}$ method and were normalized to the internal reference gene GAPDH (39).

Multiplex immunofluorescence (mIF). For the multiplex immunofluorescence (mIF) staining, tissue samples from leiomyosarcoma and fibrosarcoma tumors were used. These samples were obtained from two individual patients. This was done to ensure a diverse representation of STS subtypes in the analysis. The CFLAR mouse antibody was obtained from Santa Cruz Biotechnology, Inc. (cat. no. sc-5276). Briefly, 4-μm paraffin-embedded sections were dewaxed, and then underwent antigen retrieval, endogenous peroxidase blocking and serum blocking. The fixation information

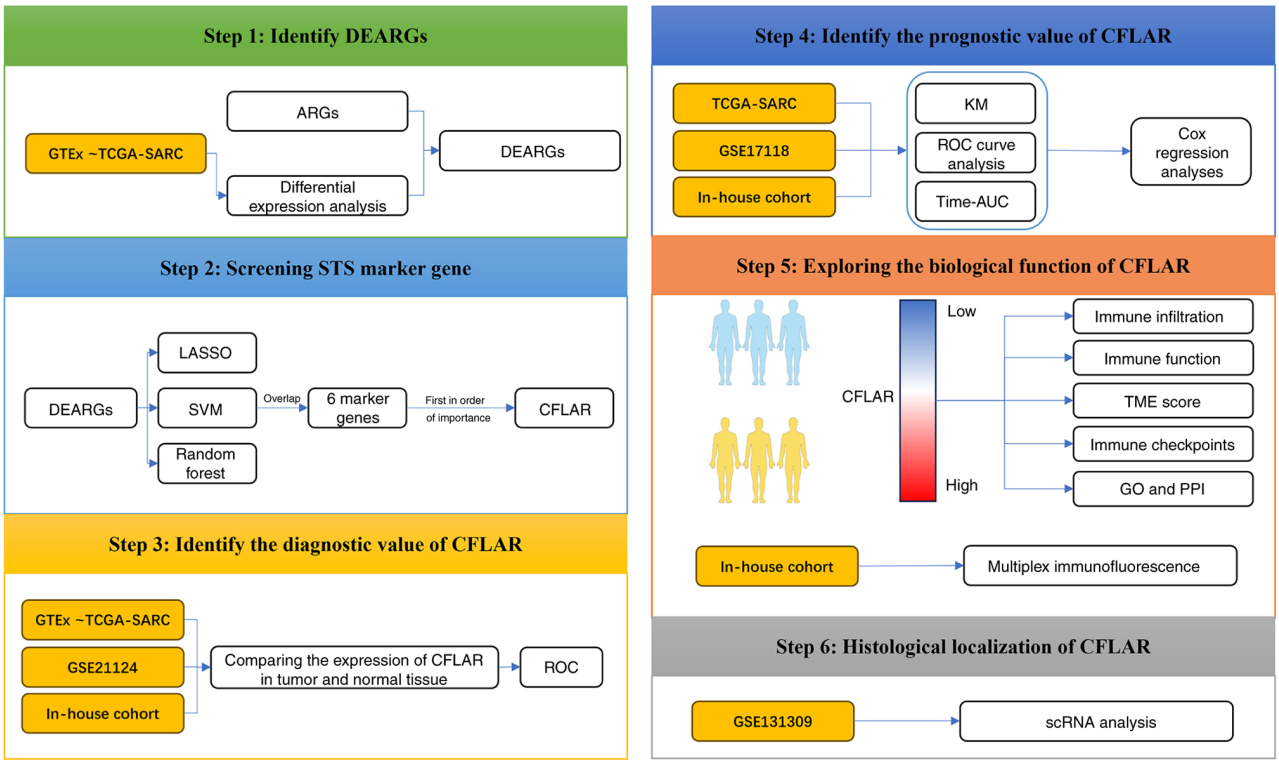

Figure 1. Flow chart of the study design. ARGs, anoikis-related genes; AUC, area under the curve; CFLAR, CASP8 and FADD-like apoptosis regulator; DEARGs, differentially expressed ARGs; GO, Gene Ontology; GTEx, Genotype-Tissue Expression; KM, Kaplan-Meier; LASSO, Least Absolute Shrinkage and Selection Operator; PPI, protein-protein interaction; ROC, receiver operating characteristic; scRNA, single cell RNA; STS, soft tissue sarcoma; SVM, Support Vector Machine; TCGA, The Cancer Genome Atlas; TME, tissue microenvironment. The human figure outline in this figure was sourced from Smart Servier Medical Art (https://smart.servier.com/). Smart Servier Medical Art provides images that are free to use and do not require permission for their usage.

for paraffin-embedded sections is as follows: The fixative used was absolute ethanol. Tissue sections were fixed at room temperature for 24 h. Antigen retrieval was carried out using citrate antigen retrieval solution (pH 6.0; Wuhan Saiwei Biotechnology Co., Ltd.), with medium heat for 8 min in citric acid, no heat for 8 min and medium-low heat for 7 min. Anjie Hi-tech 3% hydrogen peroxide was used to block endogenous peroxidase, and samples were incubated at room temperature in the dark for 25 min. Bovine serum albumin (BSA; Wuhan Saier Biotechnology Co., Ltd.) was used for serum blocking (cat. no. GC305010) at room temperature for 30 min. Subsequently, the sections were incubated with the primary antibody overnight at 4˚C. This incubation was performed three times with different antibodies: CFLAR Mouse Antibody (1:1,000; cat. no. sc-5276; Santa Cruz Biotechnology, Inc.), CD8 Rabbit Antibody (1:200; cat. no. GB12068; Wuhan Servicebio Technology Co., Ltd.) and INOS Mouse Antibody (1:200; cat. no. GB11119; Wuhan Servicebio Technology Co., Ltd.). A horseradish peroxidase-conjugated secondary antibody (HRP-conjugated Goat Anti-Mouse IgG, cat. no. GB23301; CY3-conjugated Goat Anti-Mouse IgG, cat. no. GB21301 and Alexa Fluor 488-conjugated Goat Anti-Rabbit IgG, cat. no. GB25303; all Wuhan Servicebio Technology Co., Ltd.) was applied at room temperature for 50 min, before fluorescent dye detection and microwave treatment to remove the bound antibodies. Finally, the slides were counterstained with DAPI and mounted in anti-fade solution. Imaging was performed using a Nikon Eclipse C1 upright fluorescence microscope.

Statistical analysis. All statistical analyses were performed using R statistical software (version 4.2.3). Independent samples t-test was used for comparisons between gene expression levels, and Spearman's rank correlation coefficient was carried out to assess the potential association between CFLAR expression and the infiltration of various immune-related cells. In addition, ROC curve analysis was conducted to determine the discriminatory value of marker genes. $P<0.05$ was considered to indicate a statistically significant difference.

Results

Differentially expressed ARGs (DEARGs) obtained from GTEx~TCGA-SARC. The design of the present study is shown in Fig. 1. In total, 640 ARGs were obtained from GeneCards and Harmonizome. The aforementioned genes were included in the differential expression analysis between STS and healthy tissues in GTEx~TCGA-SARC, and 86 DEARGs were obtained. The results of the differential expression analysis are displayed in heat and volcano maps (Fig. 2A and B).

Identification of diagnostic markers in STS. In total, 21 STS feature genes (those with potential to serve as diagnostic markers for STS) were obtained from DEARGs using LASSO logistic regression, 83 STS feature genes were obtained from DEARGs using SVM-REF, and 14 STS feature genes were obtained from DEARGs using RF (Fig. 2C-E). In addition, the importance of the 14 Feature genes obtained using RF was ranked (Fig. 2F). Subsequently, an intersection diagram

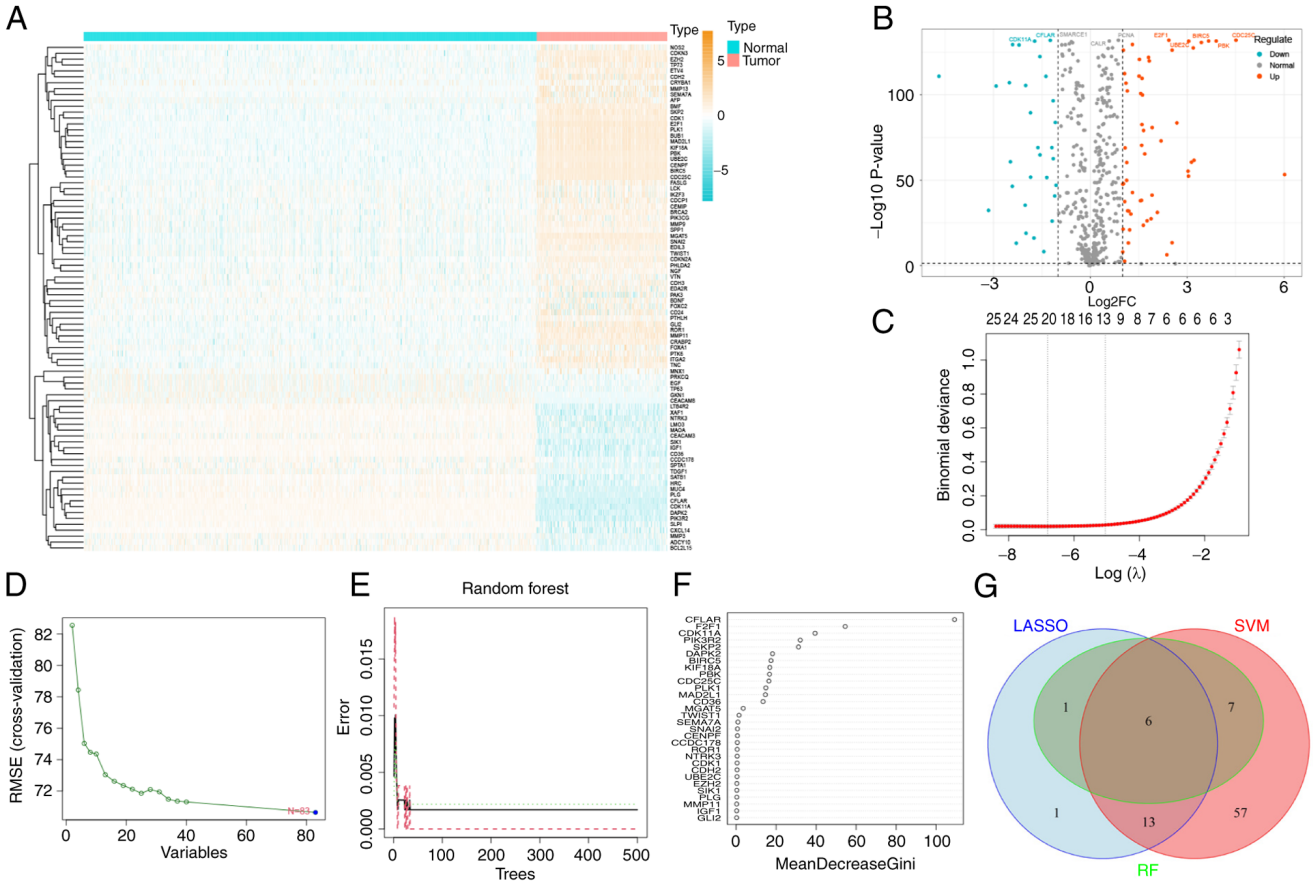

Figure 2. Differential expression analysis and three machine learning algorithms were used to screen STS biomarkers. (A) DEARG expression heatmap. (B) DEARG expression volcano map. (C) LASSO regression model was used to identify potential markers for STS. The coefficient value is displayed on the y-axis, the logarithmic value of l is displayed on the lower end of the x-axis, and the number of non-zero coefficients present in the model are displayed on the upper end of the x-axis. (D) A chart was used to demonstrate the process of selecting biomarkers through the SVM-recursive feature elimination technique. (E) A chart was used to illustrate how the number of decision trees affects the error rate. The x-axis displays the number of decision trees and the y-axis demonstrates the error rate. As the number of decision trees increases, the error rate initially decreases. When ~100 decision trees are used, the error rate remains stable. (F) The Gini coefficient method was used to determine the significance index of genetic variables. The y-axis of the chart represents the genetic variables and the x-axis demonstrates the corresponding significance index. (G) Venn diagram of the intersection of three machine learning algorithms. DEARGs, differentially expressed anoikis-related genes; LASSO, Least Absolute Shrinkage and Selection Operator; l, lamda; RF, Random Forest; STS, soft tissue sarcoma; SVM, Support Vector Machine.

between the Feature genes obtained using the three algorithms was generated, and six marker genes were obtained (Fig. 2G). Notably, CFLAR was the gene with the highest ranking of importance in RF, and this was selected for use in subsequent studies. The expression levels of CFLAR were compared between STS and healthy tissues obtained from two public datasets, GTEx~TCGA-SARC and GSE21124. The results of the present study demonstrated that the expression levels of CFLAR were significantly lower in STS tissues compared with those in healthy tissues, and the AUCs were 0.999 and 0.945, respectively (Fig. 3A-D). Subsequently, RT-qPCR was carried out to determine the relative expression levels of CFLAR in 45 tumor and 18 adjacent healthy tissues. Notably, these results were consistent with the results obtained using the public databases. The expression levels of CFLAR were significantly lower in tumor tissues compared with those in adjacent healthy tissues, and the AUC was 0.789 (Fig. 3E and F). Thus, CFLAR exhibits potential as a diagnostic marker in STS.

CFLAR is a prognostic factor in STS. The present study aimed to explore whether CFLAR plays a role in the prognosis of STS. The results of the univariate Cox regression analysis demonstrated that CFLAR was a prognostic factor for STS (Fig. 4A). Subsequently, survival analysis was conducted using the TCGA-SARC and GSE17118 datasets. Using the median CFLAR expression value in TCGA-SARC, the samples were stratified into high and low CFLAR expression groups, with the high expression group consisting of 128 samples and the low expression group also comprising 128 samples in TCGA-SARC. In the GSE17118 dataset, the high expression group included 12 samples, while the low expression group contained 25 samples. Kaplan-Meier survival curves were then generated for these groups (Fig. 4B and C). The results of the present study demonstrated that the overall survival (OS) rate of the CFLAR high expression group was significantly higher than that of the CFLAR low expression group, and the time-dependent AUC of OS was calculated (Fig. 4D and E). In TCGA-SARC, the AUC values at 1, 3 and 5 years were 0.653, 0.654 and 0.622, respectively. In the GSE17118 dataset, the AUC values at 1, 3 and 5 years were 0.824, 0.710 and 0.737, respectively. The AUC over time was plotted, and the results demonstrated that over 5 years, the AUC remained stable.

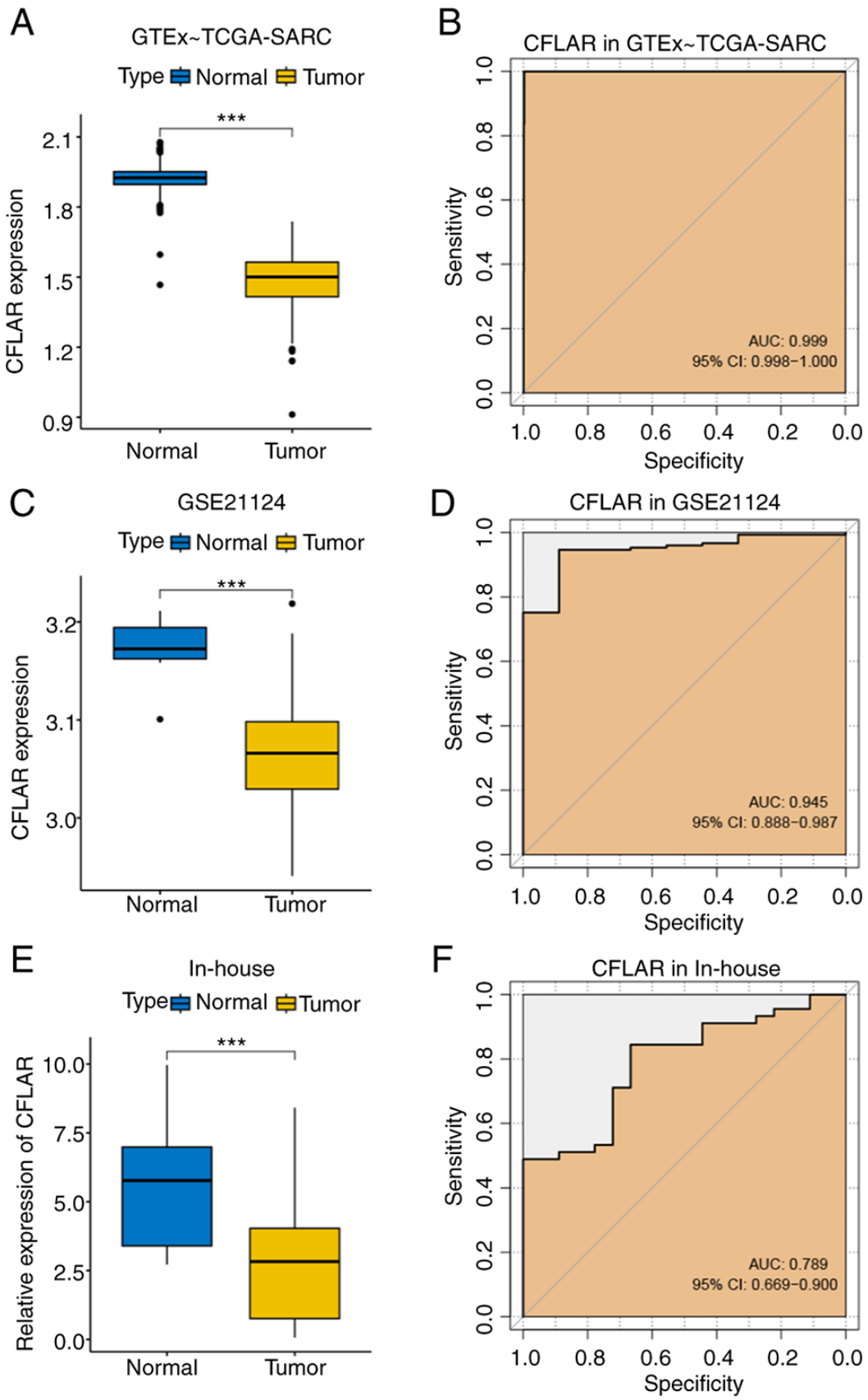

Figure 3. Identification of diagnostic markers in STS. (A) Box plot of the comparison of CFLAR expression between healthy tissues and tumor tissues in the GTEx~TCGA-SARC dataset. (B) ROC curve construction in the GTEx~TCGA-SARC dataset to evaluate the diagnostic accuracy of CFLAR in STS. (C) Box plot of the comparison of CFLAR expression between healthy tissues and tumor tissues in the GSE21124 dataset. (D) ROC curve construction in the GSE21124 dataset to evaluate the diagnostic accuracy of CFLAR in STS. (E) Box plot of the comparison of CFLAR expression between healthy tissues and tumor tissues in the in-house cohort. (F) ROC curve construction in the in-house cohort to evaluate the diagnostic accuracy of CFLAR in STS. ***P<0.001. AUC, area under the curve; CFLAR, CASP8 and FADD-like apoptosis regulator; CI, confidence interval; GTEx, Genotype-Tissue Expression; ROC, receiver operating characteristic; STS, soft tissue sarcoma; TCGA, The Cancer Genome Atlas.

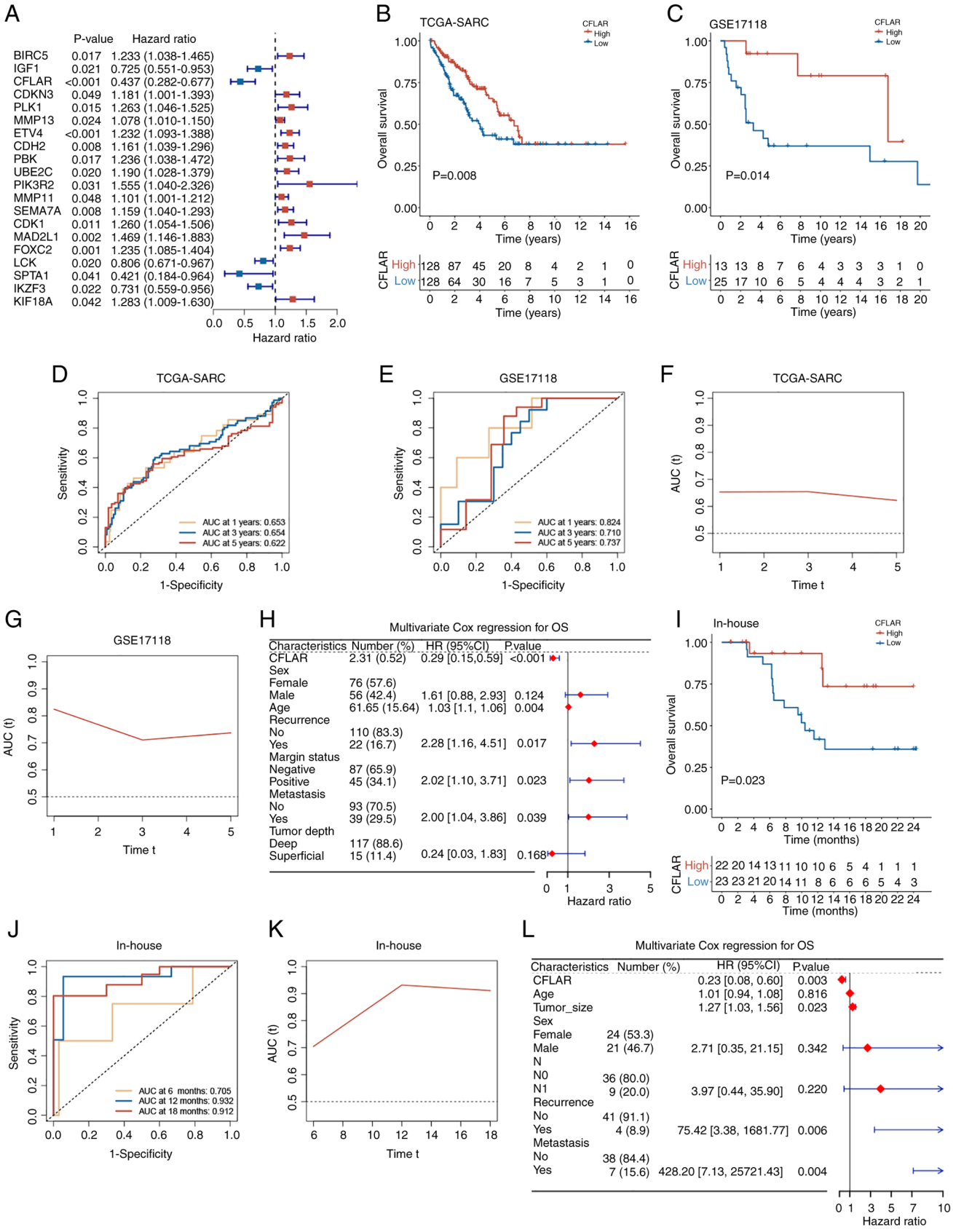

Figure 4. Impact of CFLAR on the prognosis of STS. (A) Forest plot of univariate Cox regression analysis of DEARGs. OS curves of CFLAR high and low expression groups in (B) TCGA-SARC dataset and (C) GSE17118 dataset. ROC curve construction in (D) TCGA-SARC dataset and (E) GSE17118 dataset to evaluate the accuracy of predicting 1-, 3- and 5-year survival rates. AUC over time in (F) TCGA-SARC cohort and (G) GSE17118 cohort. (H) Forest plot of multivariate Cox regression analysis of CFLAR with other clinical characteristics in TCGA-SARC cohort. (I) OS curves of CFLAR high and low expression groups in the in-house cohort. (J) ROC curve construction in the in-house cohort to evaluate the accuracy of predicting 6-, 12- and 18-month survival rates. (K) AUC over time in the in-house cohort. (L) Forest plot of multivariate Cox regression analysis of CFLAR with other clinical characteristics in in-house cohort. AUC, area under the curve; CFLAR, CASP8 and FADD-like apoptosis regulator; DEARGs, differentially expressed anoikis-related genes; OS, overall survival; ROC, receiver operating characteristic curve; STS, soft tissue sarcoma; TCGA, The Cancer Genome Atlas.

Notably, the AUC was >0.6 in TCGA-SARC cohort and >0.7 in the GSE17118 cohort (Fig. 4F and G). Subsequently, 132 patients with complete clinical information were selected from the TCGA-SARC dataset. This selection was based on the availability of comprehensive clinical data necessary for a robust multivariate Cox regression analysis. CFLAR expression was then included as a clinical feature in this analysis. The results of the present study demonstrated that CFLAR was an independent factor for the prognosis of STS (P<0.001; HR, 0.29; 95% CI, 0.15-0.59; Fig. 4H). Subsequently, the median CFLAR expression was used as a cut-off value in the in-house cohort, samples were divided into CFLAR high and low expression groups, and KM survival curves were plotted (Fig. 4I). Notably, the results were consistent with those obtained using public databases, and the time-dependent AUC of OS was calculated (Fig. 4J). The AUC values at 6, 12 and 18 months were 0.705, 0.932 and 0.912, respectively. The AUC over time demonstrated that over 1.5 years, the AUC remained stable, and was >0.7 in the in-house cohort (Fig. 4K). Subsequently, a multivariate Cox regression analysis was performed, and the clinical characteristics of the in-house cohort were incorporated. The results of the present study demonstrated that CFLAR was an independent prognostic factor for STS (P=0.003; HR, 0.23; 95% CI, 0.08-0.60; Fig. 4L). Collectively, the results of the present study demonstrated that CFLAR may exhibit potential as an independent prognostic factor for STS.

Immune cell infiltration, immune function, TME score and ICI analysis. To further explore the role of high CFLAR expression in improving prognosis, immune cell infiltration analysis was performed using CIBERSORTx. The results of the present study demonstrated that the infiltration of $CD8^+$ T cells, monocytes and M1 macrophages was significantly higher in the CFLAR high expression group than that in the low expression group, whereas M0 macrophage infiltration was significantly lower in the CFLAR high expression group than that in the low expression group. In addition, the γδT cells in the CFLAR high expression group were higher than those in the low expression group (Fig. 5A).

Correlation analysis of immune cell infiltration demonstrated that CFLAR expression was most notably and positively correlated with $CD8^+$ T cells, M1 macrophages and monocytes, and negatively correlated with M0 macrophages. While a positive correlation was also observed with γδT cells and Tregs, these associations were characterized by a lower r-value (<0.3), indicating a weaker relationship (Fig. 5B). The correlation, correlation coefficient and P-value of CFLAR expression and immune cell infiltration are summarized in a lollipop chart (Fig. 5C). Thus, it was hypothesized that CFLAR may promote the infiltration of $CD8^+$ T cells and the polarization of M1 macrophages in the STS TME.

The results of the immune function analysis demonstrated that the majority of immune function scores were significantly higher in the CFLAR high expression group than those in the CFLAR low expression group (Fig. 5D). The results of the TME analysis demonstrated that the StromalScore, ImmuneScore and ESTIMATEScore in the CFLAR high expression group were significantly higher than those in the CFLAR low expression group (Fig. 5E). Moreover, to explore the role of CFLAR in predicting the therapeutic efficacy of ICIs, the correlation of CFLAR expression with 29 ICI targets was determined. The results are displayed in a heatmap (Fig. 5F). The results showed that CFLAR was positively correlated with most ICIs and negatively correlated with CD274. Notably, CFLAR expression may exhibit potential in guiding the immunotherapy of STS.

Functional analysis of CFLAR co-upregulated genes. To further explore how CFLAR induces the TME activation of STS, differential expression analysis was performed using both high and low CFLAR expression groups. The results of the present study demonstrated that the majority of CFLAR co-upregulated genes were highly associated with immune response, and were positive regulators of immune cell activation, immune receptor activation and immune pathway activation (Fig. 6A). Subsequently, the PPI network of CFLAR co-upregulated genes was generated (Fig. 6B). The results of the present study demonstrated that all hub genes in the PPI network were immune-related genes, and these were associated with immune cell activation and antigen presentation.

Single-cell sequencing analysis and CFLAR expression distribution. Following quality control of the GSE131309 single-cell sequencing dataset, data dimensionality reduction was performed using the UMAP method, and all cells were divided into 20 clusters (Fig. 6C). In addition, results of the cell annotation demonstrated that annotated cell types were monocytes/macrophages, $CD8^+$ T cells, $CD4^+$ T cells, B cells, fibroblasts, sarcoma cells, vascular endothelial cells and mastocytes (Fig. 6D). The results of the present study also demonstrated that CFLAR expression was higher in non-tumor tissues than in tumor tissues, and CFLAR was mainly expressed in T cells and monocytes/macrophages (Fig. 6E). Thus, the results obtained using RNA-seq data were further verified at the single-cell level.

CFLAR promotes infiltration of $CD8^+$ T cells and M1 macrophages. To further verify the results of the immune cell infiltration analysis, mIF staining was performed using tumor tissues of patients with STS. The results of the present study demonstrated that the infiltration of $CD8^+$ T cells and M1 macrophages was markedly increased in tumor tissues when CFLAR expression was high (Fig. 7A and B). Collectively, the results of the present study highlighted that CFLAR was associated with the infiltration of $CD8^+$ T cells and the polarization of M1 macrophages.

Discussion

Anoikis was initially used to describe a particular phenomenon that occurs when a cell undergoes apoptotic cell death as a result of inadequate interactions with the ECM (40,41). Subsequently, it was discovered that this distinct form of cell death serves a crucial role in tumor angiogenesis and metastasis, and exerts a significant impact on tumor prognosis (40-42). Healthy epithelial and endothelial cells detach and undergo anoikis to prevent the growth of cells that have been oncogenically transformed. However, tumor cells may acquire resistance to this process, which allows them to migrate to other sites in the

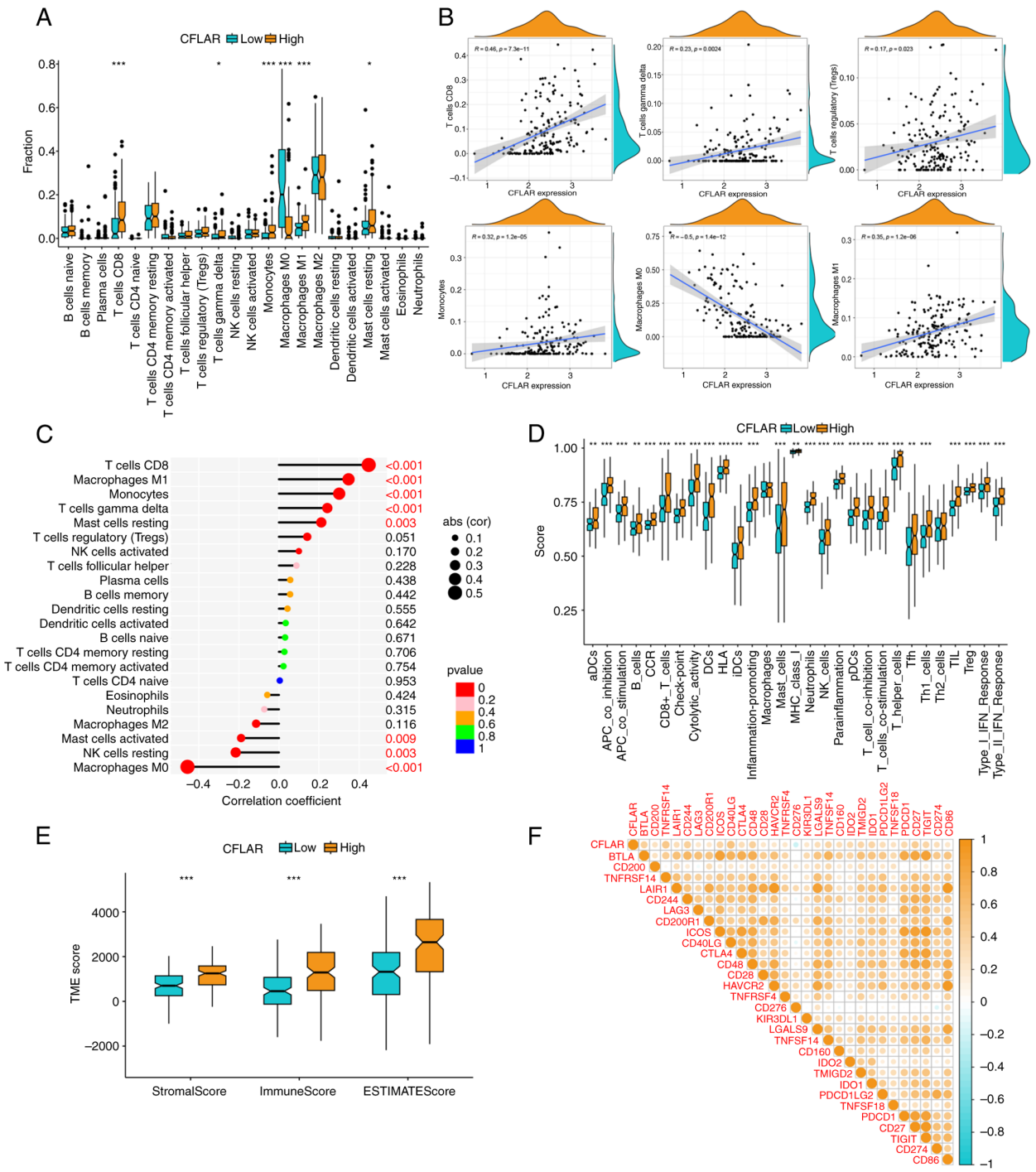

Figure 5. Immune cell infiltration, immune function, TME score and ICI correlation analysis. (A) A boxplot illustrating the proportion of 22 types of immune cells in CFLAR high and low expression groups. (B) Correlation analysis between CFLAR expression and infiltration of CD8$^+$ T cells, γδT cells, M1 macrophages, M0 macrophages, monocytes and Treg. (C) A lollipop chart showing the correlation coefficient and significance of CFLAR expression and immune cell infiltration. (D) A boxplot illustrating the immune function scores in the CFLAR high and low expression groups. (E) A boxplot illustrating the TME scores in CFLAR high and low expression groups. (F) Correlation heatmap between CFLAR and 29 ICIs. *P<0.05, **P<0.01, ***P<0.001. CFLAR, CASP8 and FADD-like apoptosis regulator; ICI, immune checkpoint inhibitor; NK, natural killer; TME, tumor microenvironment.

body and form metastatic tumors. This ability to evade anoikis is a key factor in the progression of cancer (42). Therefore, clarifying the molecular mechanisms of anoikis and exploring novel targets for tumor treatment are required.

At present, research is focused on the molecular mechanisms of anoikis in various types of cancer, including osteosarcoma; however, studies focused on the role of anoikis in STS are rare (11,43,44). Therefore, the present study aimed to explore the diagnostic and prognostic value of ARGs in STS, and to explore their regulatory effect on the TME of STS.

Using three machine learning algorithms, LASSO, RF and SVM, STS Feature genes with the highest importance were screened from DEARGs. CFLAR, which is also referred to as c-FLIP, Casper, iFLICE, FLAME-1, CASJ, CLARP, MRIT or usurpin, has a significant role as a negative regulator of the apoptotic pathway (45). The results of a previous

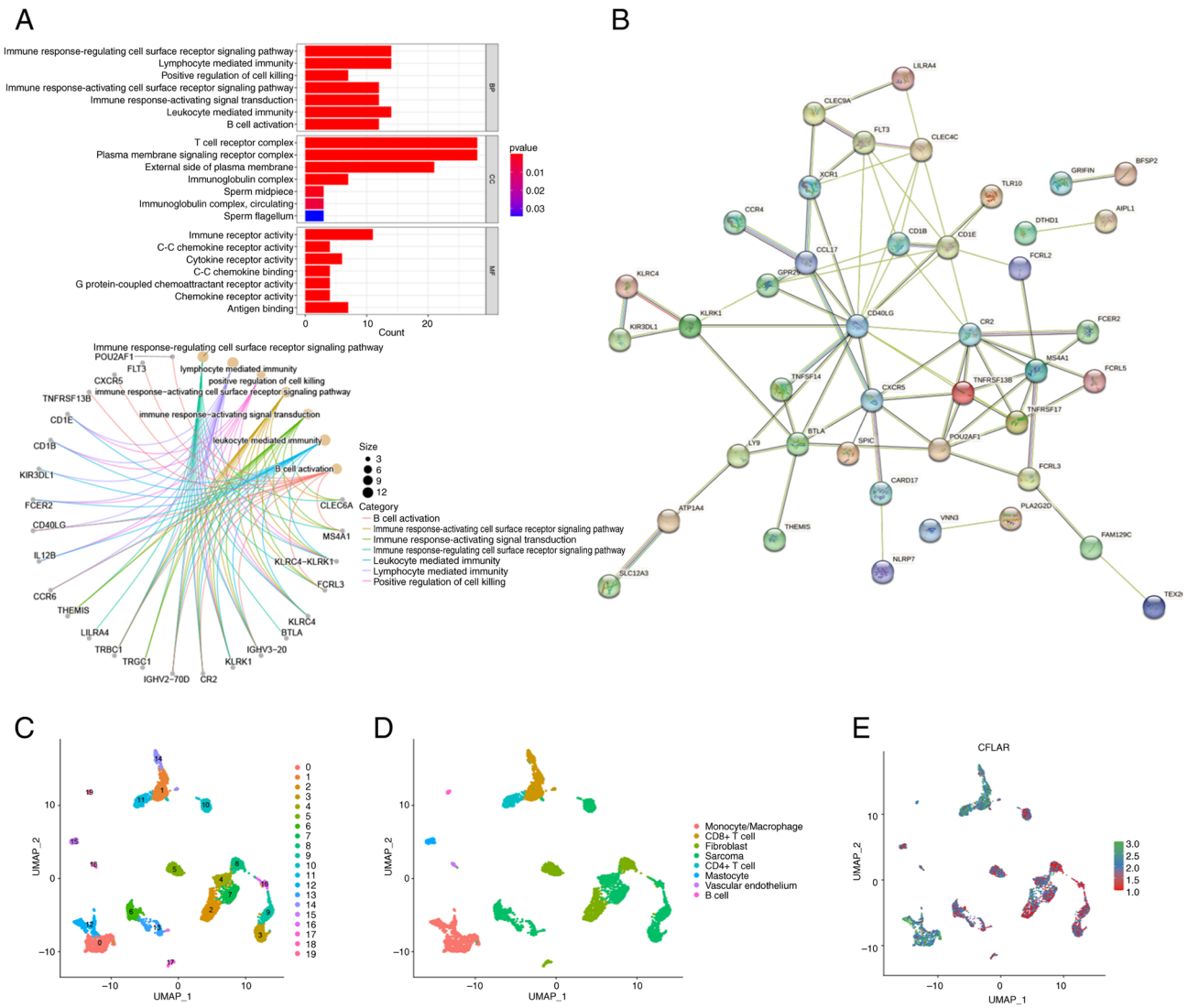

Figure 6. GO, PPI and single-cell sequencing analysis. (A) GO enrichment analysis for CFLAR co-upregulated genes. (B) PPI network of CFLAR co-upregulated genes. (C) Dimensionality reduction map of cells in the GSE131309 dataset was divided into 20 clusters using UMAP. (D) Cells in the GSE131309 dataset were annotated as follows: Monocytes/macrophages, $CD8^+$ T cells, $CD4^+$ T cells, B cells, fibroblasts, sarcoma cells, vascular endothelial cells and mastocytes. (E) CFLAR was mainly expressed in T cells and monocytes/macrophages in the STS TME. CFLAR, CASP8 and FADD-like apoptosis regulator; GO, Gene Ontology; PPI, protein-protein interaction; STS, soft tissue sarcoma; TME, tumor microenvironment; UMAP, uniform manifold approximation and projection.

study demonstrated that recruitment of CFLAR to either the death-inducing signaling complex or complex II prevents procaspase-8 dimerization and activation. As a result, the activation of the apoptotic cascade is blocked, which may protect the cell from ligand-mediated death (16).

The results of cell line studies demonstrated that levels of CFLAR are higher in various types of cancer, including colorectal carcinoma, gastric adenocarcinoma, pancreatic carcinoma, melanoma, ovarian carcinoma and prostate carcinoma (46-51). However, the results of the present study demonstrated that the expression levels of CFLAR in STS were significantly lower than those in healthy tissues.

Moreover, the results of a previous study demonstrated that high CFLAR expression may induce anti-apoptotic effects in tumor cells, thereby leading to their avoidance of apoptosis and tumor development (52). Therefore, the association between CFLAR and STS prognosis was examined; the present study demonstrated that low CFLAR expression in STS was associated with a poor prognosis, which differs from the results obtained in different cancer types (53-57).

The present study aimed to explore the role of CFLAR expression in STS tissues, and the association between high CFLAR expression and prognosis. The results of the present study demonstrated that high CFLAR expression could promote immune cell infiltration and immune response in the STS TME. The majority of the genes co-upregulated with CFLAR were enriched in immune-related functions, and hub genes, such as TNFRSF13B, CXCR5, CD40LG, CR2, MS4A1, TNFRSF17, POU2AF1, CD1E, CD1B, CCL17 and FLT3, were associated with immune cell activation and antigen presentation. The results of the single-cell sequencing analysis demonstrated that CFLAR was highly expressed in immune cells. Therefore, it was hypothesized that CFLAR may be associated with immune response.

The results of previous studies have demonstrated that CFLAR plays an important role in the regulation of T cells.

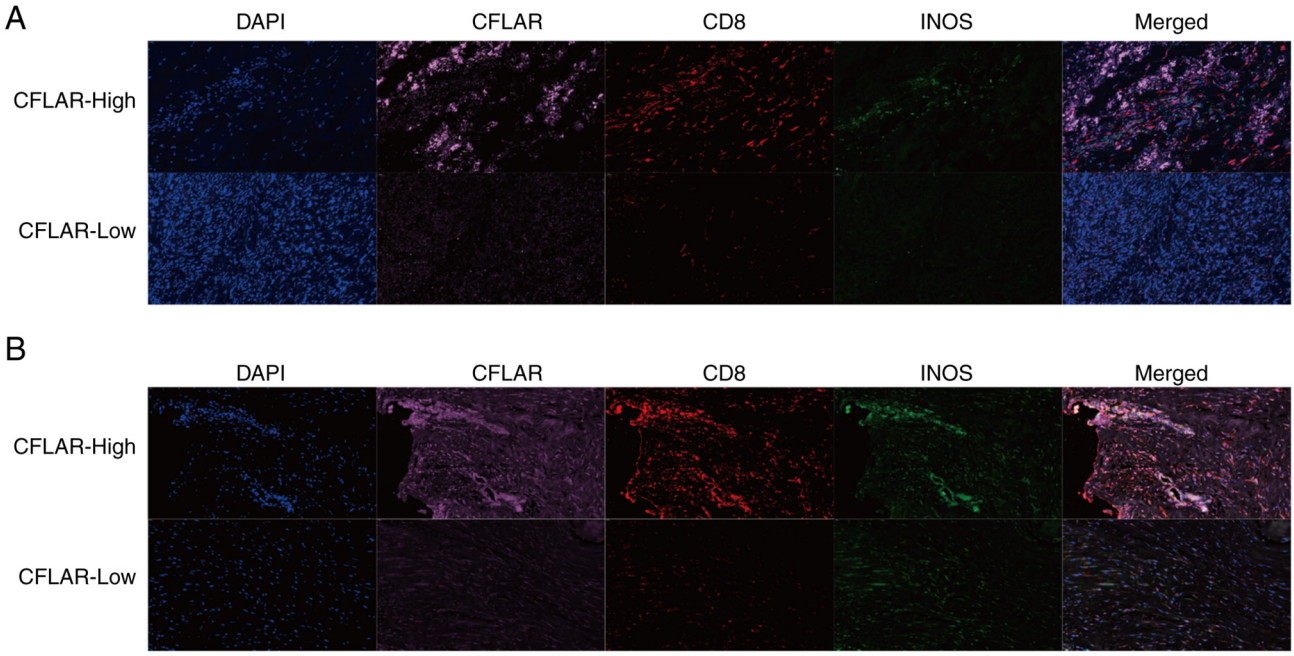

Figure 7. CFLAR promotes infiltration of CD8$^+$ T cells and M1 macrophages. Multiple immunofluorescence staining of CFLAR, CD8 and INOS in (A) leiomyosarcoma tumor tissue and (B) fibrosarcoma tumor tissue, with images captured at x20 magnification. CFLAR, CASP8 and FADD-like apoptosis regulator; INOS, inducible nitric oxide synthase.

Notably, CFLAR is required for the survival and proliferation of T cells, and the expansion of T cells in response to T-cell receptor (TCR) stimulation (58,59). The presence of CFLAR not only ensures the survival of T cells with or without TCR activation, but also promotes the regular circulation of T cells upon stimulation (58). The results of a previous study also demonstrated that CFLAR exerts a significant effect on the activation of T cells. Notably, Jurkat T cells overexpressing CFLAR have been shown to produce higher levels of IL-2 following TCR stimulation than wild-type Jurkat T cells. Examination of the pathways that regulate IL-2 expression revealed that TCR-mediated activation of NF-κB and mitogen-activated protein kinase (MAPK)/extracellular-regulated protein kinase (ERK) was augmented in the presence of increased CFLAR expression (60). Further investigations into these pathways demonstrated that CFLAR is associated with tumor necrosis factor receptor-associated factor (TRAF)1, TRAF2 and receptor-interacting protein 1 (RIP1), which together promote NF-κB activation. These proteins are also associated with RAF1, which activates ERK through MAPK/ERK kinase (MEK)1 and MEK2 (59). In conclusion, CFLAR may promote the activation of T cells, which in turn increases the immune response in the STS TME.

The results of a previous study demonstrated that monocytes undergo transformation into macrophages in the peripheral blood. During this process, monocytes contain low levels of CFLAR and are highly sensitive to CD95-induced cell death. By contrast, macrophages express high levels of CFLAR and are resistant to CD95-induced cell death, despite high levels of CD95 expression on the cell surface (59). In addition, it has been demonstrated that the activation of caspase-8 is required for blood monocytes to become macrophages. When primary monocytes are exposed to macrophage colony-stimulating factor or when U937 cells are exposed to tissue polypeptide antigen, caspase-8 interacts with FADD, FLIP and RIP1. This multi-molecular platform activates caspase-8, which results in the cleavage of RIP1. The cleavage fragments of RIP1 may reduce the activity of NF-κB, which leads to the differentiation of monocytes into macrophages (61). Moreover, the results of a previous study demonstrated that CFLAR protects macrophages from lipopolysaccharide-induced pyroptosis via inhibition of complex II formation (62). The aforementioned studies revealed that CFLAR inhibits the apoptosis of macrophages through specific mechanisms, which may explain the positive correlation between the expression of CFLAR in the STS TME, and the infiltration of M1 macrophages and monocytes observed in the present study.

Notably, CFLAR is closely associated with the activation of T cells and the maintenance of macrophage activity, which increases the immune response in the STS TME. The role of CFLAR in different cancer types remains unclear. On the one hand, CFLAR may inhibit the apoptosis of tumor cells, and on the other hand, CFLAR may promote the immune response in the STS TME. Therefore, it was hypothesized that the main role of CFLAR may differ between cancer types. For example, in other cancer types, CFLAR mainly inhibits the apoptosis of tumor cells; however, it does not significantly promote the immune response. By contrast, the results of the present study demonstrated that CFLAR mainly promoted the immune response in the STS TME, whereas the inhibition of STS cell apoptosis was not observed. As a result, CFLAR expression is often increased in other types of cancer tissues, and the corresponding overexpression indicates a poor prognosis. Notably, the opposite results were observed in STS, and further investigations are required.

Collectively, the results of the present study revealed the diagnostic and prognostic value of CFLAR in STS, and explored the regulatory effects on the STS TME. However, the present study has several limitations. As STS is rare, the sample

size included in the present study was limited. In addition, patient survival was only followed up for 2 years, meaning that the effects of CFLAR on the 5-year survival rate of patients were not verified. In addition, immunohistochemical data for STS were limited. Experiments involving cell lines, organoids and animals were not conducted; thus, further *in vivo* and *in vitro* investigations are required to determine the specific mechanisms of action of CFLAR in STS.

In conclusion, CFLAR exhibits potential as a biomarker for the prediction of STS progression and disease outcomes. In addition, the results of the present study highlighted that CFLAR may serve a crucial role in determining the immune response to STS, as it enhances the infiltration of $CD8^+$ T cells and M1 macrophages, which are key immune cells that aid in the elimination of cancer cells. Collectively, the results of the present study suggested that CFLAR may exhibit potential as a therapeutic target in the treatment of STS.

Acknowledgements

The human figure outline in Fig. 1 was sourced from Smart Servier Medical Art (https://smart.servier.com/), used under a Creative Commons Attribution 3.0 Unported License (https://creativecommons.org/licenses/by/3.0/). No modifications were made to the image.

Funding

This study was supported by the National Natural Science Foundation of China (grant nos. 82002848 and 82272964); the CAMS Innovation Fund for Medical Sciences (grant nos. 2021-I2M-C&T-B-054 and 2021-I2M-C&T-B-053); the Capital Characterized Clinical Application Research Fund of Beijing Municipal Science and Technology Commission of China (grant no. Z171100001017210); the Fundamental Research Funds for the Central Universities (grant no. 3332021097); and the Beijing Hope Run Special Fund of Cancer Foundation of China (grant no. LC2021A1).

Availability of data and materials

The data generated in the present study may be found in TCGA, GTEx and GEO databases under accession numbers TCGA-SARC, GSE17118, GSE21124 and GSE131309 or at the following URLs: TCGA-SARC, https://xenabrowser.net/datapages/?cohort=GDC%20TCGA%20Sarcoma%20(SARC)&removeHub=https%3A%2F%2Fxena.treehouse.gi.ucsc.edu%3A443; GTEx, https://xenabrowser.net/datapages/?cohort=GTEX&removeHub=https%3A%2F%2Fxena.treehouse.gi.ucsc.edu%3A443; GSE17118, https://www.ncbi.nlm.nih.gov/geo/query/acc.cgi?acc=GSE17118; GSE21124, https://www.ncbi.nlm.nih.gov/geo/query/acc.cgi?acc=GSE21124; and GSE131309, https://www.ncbi.nlm.nih.gov/geo/query/acc.cgi?acc=GSE131309.

Authors' contributions

XuL analyzed the data, wrote and revised the manuscript, and spearheaded the verification experiments. SY conceptualized and oversaw the entire project. XuL and SY confirm the authenticity of all the raw data. XiL provided project supervision, participated in data analysis and discussion, and contributed to manuscript revisions. All authors read and approved the final manuscript.

Ethics approval and consent to participate

All tissue samples used in the present study were reviewed by the institutional ethics committee, and all patients provided written informed consent. The ethics approval for the present study was granted by the Institutional Review Board of National Cancer Center/National Clinical Research Center for Cancer/Cancer Hospital, Chinese Academy of Medical Sciences and Peking Union Medical College (approval no. NCC2020C-341; Beijing, China). All patients who provided specimens for this study gave written informed consent for their participation.

Patient consent for publication

All patients who provided specimens for this study gave written informed consent for the publication of results derived from their specimens, in compliance with ethical standards and respect for patient confidentiality and privacy.

Competing interests

The authors declare that they have no competing interests.

Use of artificial intelligence tools

During the preparation of this work, the authors used ChatGPT 3.5 in order to improve the readability and language of the article. Subsequently, the authors revised and edited the content produced by the AI tools as necessary, taking full responsibility for the ultimate content of the present manuscript.

References

1. Gamboa AC, Gronchi A and Cardona K: Soft-tissue sarcoma in adults: An update on the current state of histiotype-specific management in an era of personalized medicine. CA Cancer J Clin 70: 200-229, 2020.
2. Vilanova JC: WHO classification of soft tissue tumors. In: Imaging of Soft Tissue Tumors. Vanhoenacker F, Parizel P, Gielen J (eds). 4th Edition, Springer, Cham, Switzerland, pp 187-196, 2017.
3. Hoven-Gondrie ML, Bastiaannet E, Ho VKY, van Leeuwen BL, Liefers GJ, Hoekstra HJ and Suurmeijer AJ: Worse survival in elderly patients with extremity soft-tissue sarcoma. Ann Surg Oncol 23: 2577-2585, 2016.
4. Crago AM and Brennan MF: Principles in management of soft tissue sarcoma. Adv Surg 49: 107-122, 2015.
5. Navarria P, Ascolese AM, Cozzi L, Tomatis S, D'Agostino GR, De Rose F, De Sanctis R, Marrari A, Santoro A, Fogliata A, *et al*: Stereotactic body radiation therapy for lung metastases from soft tissue sarcoma. Eur J Cancer 51: 668-674, 2015.
6. Sameer UK, Kaneez F and Fayaz M: Understanding the cell survival mechanism of anoikis-resistant cancer cells during different steps of metastasis. Clin Exp Metastasis 39: 715-726, 2022.
7. Gilmore AP: Anoikis. Cell Death Differ 12: 1473-1477, 2005.
8. Weiss F, Lauffenburger D and Friedl P: Towards targeting of shared mechanisms of cancer metastasis and therapy resistance. Nat Rev Cancer 22: 157-173, 2022.
9. Berezovskaya O, Schimmer AD, Glinskii AB, Pinilla C, Hoffman RM, Reed JC and Glinsky GV: Increased expression of apoptosis inhibitor protein XIAP contributes to anoikis resistance of circulating human prostate cancer metastasis precursor cells. Cancer Res 65: 2378-2386, 2005.

10. Kim YN, Koo KH, Sung JY, Yun UJ and Kim H: Anoikis resistance: An essential prerequisite for tumor metastasis. Int J Cell Biol 2012: 306879, 2012.
11. Yu Y, Song Y, Cheng L, Chen L, Liu B, Lu D, Li X, Li Y, Lv F and Xing Y: CircCEMIP promotes anoikis-resistance by enhancing protective autophagy in prostate cancer cells. J Exp Clin Cancer Res 41: 188, 2022.
12. Fulda S: Targeting c-FLICE-like inhibitory protein (CFLAR) in cancer. Expert Opin Ther Targets 17: 195-201, 2013.
13. Irmler M, Thome M, Hahne M, Schneider P, Hofmann K, Steiner V, Bodmer JL, Schröter M, Burns K, Mattmann C, *et al*: Inhibition of death receptor signals by cellular FLIP. Nature 388: 190-195, 1997.
14. Xiaohong W, Jun Z, Hongmei G and Fan Q: CFLAR is a critical regulator of cerebral ischaemia-reperfusion injury through regulating inflammation and endoplasmic reticulum (ER) stress. Biomed Pharmacother 117: 109155, 2019.
15. Xiao J, Moon M, Yan L, Nian M, Zhang Y, Liu C, Lu J, Guan H, Chen M, Jiang D, *et al*: Cellular FLICE-inhibitory protein protects against cardiac remodelling after myocardial infarction. Basic Res Cardiol 107: 239, 2012.
16. Shirley S and Micheau O: Targeting c-FLIP in cancer. Cancer Lett 332: 141-150, 2013.
17. Rao-Bindal K, Rao CK, Yu L and Kleinerman ES: Expression of c-FLIP in pulmonary metastases in osteosarcoma patients and human xenografts. Pediatr Blood Cancer 60: 575-579, 2013.
18. Lafferty-Whyte K, Bilsland A, Hoare SF, Burns S, Zaffaroni N, Cairney CJ and Keith WN: TCEAL7 inhibition of c-Myc activity in alternative lengthening of telomeres regulates hTERT expression. Neoplasia 12: 405-414, 2010.
19. Barretina J, Taylor BS, Banerji S, Ramos AH, Lagos-Quintana M, Decarolis PL, Shah K, Socci ND, Weir BA, Ho A, *et al*: Subtype-specific genomic alterations define new targets for soft-tissue sarcoma therapy. Nat Genet 42: 715-721, 2010.
20. Jerby-Arnon L, Neftel C, Shore ME, Weisman HR, Mathewson ND, McBride MJ, Haas B, Izar B, Volorio A, Boulay G, *et al*: Opposing immune and genetic mechanisms shape oncogenic programs in synovial sarcoma. Nat Med 27: 289-300, 2021.
21. Ritchie ME, Phipson B, Wu D, Hu Y, Law CW, Shi W and Smyth GK: limma powers differential expression analyses for RNA-sequencing and microarray studies. Nucleic Acids Res 43: e47, 2015.
22. Friedman J, Hastie T and Tibshirani R: Regularization paths for generalized linear models via coordinate descent. J Stat Softw 33: 1-22, 2010.
23. Wang H, Yang F and Luo Z: An experimental study of the intrinsic stability of random forest variable importance measures. BMC Bioinformatics 17: 60, 2016.
24. Huang S, Cai N, Pacheco PP, Narrandes S, Wang Y and Xu W: Applications of support vector machine (SVM) learning in cancer genomics. Cancer Genomics Proteomics 15: 41-51, 2018.
25. Tay JK, Narasimhan B and Hastie T: Elastic net regularization paths for all generalized linear models. J Stat Softw 106: 1, 2023.
26. Liaw A and Wiener M: Classification and regression by randomForest. R News 2: 18-22, 2002.
27. Meyer D, Dimitriadou E, Hornik K, Weingessel A and Leisch F: e1071: Misc functions of the department of statistics, probability theory group (Formerly: E1071), TU Wien. R package version 1.7-13. 2023.
28. Therneau TM and Grambsch PM: Modeling survival data: Extending the cox model. New York: Springer; 2000. ISBN 0-387-98784-3.
29. Kassambara A, Kosinski M and Biecek P: survminer: Drawing survival curves using 'ggplot2'. R package version 0.4.9. 2021.
30. Blanche P, Dartigues JF and Jacqmin-Gadda H: Estimating and comparing time-dependent areas under receiver operating characteristic curves for censored event times with competing risks. Stat Med 32: 5381-5397, 2013.
31. Kassambara A: ggpubr: 'ggplot2' Based Publication Ready Plots. R package version 0.6.0. 2023.
32. Hänzelmann S, Castelo R and Guinney A: GSVA: Gene set variation analysis for microarray and RNA-seq data. BMC Bioinformatics 14: 7, 2013.
33. Yoshihara K, Kim H and Verhaak RG: Estimate of stromal and immune cells in malignant tumor tissues from expression data. R package version 1.0.13/r21. 2016.
34. Wu T, Hu E, Xu S, Chen M, Guo P, Dai Z, Feng T, Zhou L, Tang W, Zhan L, *et al*: ClusterProfiler 4.0: A universal enrichment tool for interpreting omics data. The Innovation 2: 100141, 2021.
35. Gentleman RC, Carey VJ, Bates DM, Bolstad B, Dettling M, Dudoit S, Ellis B, Gautier L, Ge Y, Gentry J, *et al*: Bioconductor: Open software development for computational biology and bioinformatics. Genome Biol 5: R80, 2005.
36. Stuart T, Butler A, Hoffman P, Hafemeister C, Papalexi E, Mauck WM III, Hao Y, Stoeckius M, Smibert P and Satija R: Comprehensive integration of single-cell data. Cell 177: 1888-1902, 2019.
37. Jerby-Arnon L, Neftel C, Shore ME, Weisman HR, Mathewson ND, McBride MJ, Haas B, Izar B, Volorio A, Boulay G, *et al*: Opposing immune and genetic mechanisms shape oncogenic programs in synovial sarcoma. Nat Med 27: 289-300, 2021.
38. Hu C, Li T, Xu Y, Zhang X, Li F, Bai J, Chen J, Jiang W, Yang K, Ou Q, *et al*: CellMarker 2.0: An updated database of manually curated cell markers in human/mouse and web tools based on scRNA-seq data. Nucleic Acids Res 51: D870-D876, 2023.
39. Livak KJ and Schmittgen TD: Analysis of relative gene expression data using real-time quantitative PCR and the 2(-Delta Delta C(T)) method. Methods 25: 402-408, 2001.
40. Frisch SM and Ruoslahti E: Integrins and anoikis. Curr Opin Cell Biol 9: 701-706, 1997.
41. Frisch SM and Screaton RA: Anoikis mechanisms. Curr Opin Cell Biol 13: 555-562, 2001.
42. Rennebeck G, Martelli M and Kyprianou N: Anoikis and survival connections in the tumor microenvironment: Is there a role in prostate cancer metastasis? Cancer Res 65: 11230-11235, 2005.
43. Chen Y, Huang W, Ouyang J, Wang J and Xie Z: Identification of anoikis-related subgroups and prognosis model in liver hepatocellular carcinoma. Int J Mol Sci 24: 2862, 2023.
44. Zhang Z, Zhu Z, Fu J, Liu X, Mi Z, Tao H and Fan H: Anoikis patterns exhibit distinct prognostic and immune landscapes in osteosarcoma. Int Immunopharmacol 115: 109684, 2023.
45. Micheau O: Cellular FLICE-inhibitory protein: An attractive therapeutic target? Expert Opin Ther Targets 7: 559-573, 2003.
46. Hernandez A, Wang QD, Schwartz SA and Evers BM: Sensitization of human colon cancer cells to TRAIL-mediated apoptosis. J Gastrointest Surg 5: 56-65, 2001.
47. Nam SY, Jung GA, Hur GC, Chung HY, Kim WH, Seol DW and Lee BL: Upregulation of FLIP(S) by Akt, a possible inhibition mechanism of TRAIL-induced apoptosis in human gastric cancers. Cancer Sci 94: 1066-1073, 2003.
48. Elnemr A, Ohta T, Yachie A, Kayahara M, Kitagawa H, Fujimura T, Ninomiya I, Fushida S, Nishimura GI, Shimizu K and Miwa K: Human pancreatic cancer cells disable function of Fas receptors at several levels in Fas signal transduction pathway. Int J Oncol 18: 311-316, 2001.
49. Griffith TS, Chin WA, Jackson GC, Lynch DH and Kubin MZ: Intracellular regulation of TRAIL-induced apoptosis in human melanoma cells. J Immunol 161: 2833-2840, 1998.
50. Xiao CW, Yan X, Li Y, Reddy SAG and Tsang BK: Resistance of human ovarian cancer cells to tumor necrosis factor alpha is a consequence of nuclear factor kappaB-mediated induction of Fas-associated death domain-like interleukin-1beta-converting enzyme-like inhibitory protein. Endocrinology 144: 623-630, 2003.
51. Zhang X, Jin TG, Yang H, DeWolf WC, Khosravi-Far R and Olumi AF: Persistent c-FLIP(L) expression is necessary and sufficient to maintain resistance to tumor necrosis factor-related apoptosis-inducing ligand-mediated apoptosis in prostate cancer. Cancer Res 64: 7086-7091, 2004.
52. Wang L, Jin H, Jochems F, Wang S, Lieftink C, Martinez IM, De Conti G, Edwards F, de Oliveira RL, Schepers A, *et al*: cFLIP suppression and DR5 activation sensitize senescent cancer cells to senolysis. Nat Cancer 3: 1284-1299, 2022.
53. Ullenhag GJ, Mukherjee A, Watson NFS, Al-Attar AH, Scholefield JH and Durrant LG: Overexpression of FLIPL is an independent marker of poor prognosis in colorectal cancer patients. Clin Cancer Res 13: 5070-5075, 2007.
54. Wang W, Wang S, Song X, Sima N, Xu X, Luo A, Chen G, Deng D, Xu Q, Meng L, *et al*: The relationship between c-FLIP expression and human papillomavirus E2 gene disruption in cervical carcinogenesis. Gynecol Oncol 105: 571-577, 2007.
55. Valnet-Rabier MB, Challier B, Thiebault S, Angonin R, Margueritte G, Mougin C, Kantelip B, Deconinck E, Cahn JY and Fest T: c-Flip protein expression in Burkitt's lymphomas is associated with a poor clinical outcome. Br J Haematol 128: 767-773, 2005.
56. Valente G, Manfroi F, Peracchio C, Nicotra G, Castino R, Nicosia G, Castino R, Nicosia G, Kerim S and Isidoro C: cFLIP expression correlates with tumour progression and patient outcome in non-Hodgkin lymphomas of low grade of malignancy. Br J Haematol 132: 560-570, 2006.

57. Korkolopoulou P, Goudopoulou A, Voutsinas G, Thomas-Tsagli E, Kapralos P, Patsouris E and Saetta AA: c-FLIP expression in bladder urothelial carcinomas: Its role in resistance to Fas-mediated apoptosis and clinicopathologic correlations. Urology 63: 1198-1204, 2004.
58. Chau H, Wong V, Chen NJ, Huang HL, Lin WJ, Mirtsos C, Elford AR, Bonnard M, Wakeham A, You-Ten AI, *et al*: Cellular FLICE-inhibitory protein is required for T cell survival and cycling. J Exp Med 202: 405-413, 2005.
59. Budd RC, Yeh WC and Tschopp J: cFLIP regulation of lymphocyte activation and development. Nat Rev Immunol 6: 196-204, 2006.
60. Kataoka T, Budd RC, Holler N, Thome M, Martinon F, Irmler M, Burns K, Hahne M, Kennedy N, Kovacsovics M and Tschopp J: The caspase-8 inhibitor FLIP promotes activation of NF-kappaB and Erk signaling pathways. Curr Biol 10: 640-648, 2000.
61. Rébé C, Cathelin S, Launay S, Filomenko R, Prévotat L, L'Ollivier C, Gyan E, Micheau O, Grant S, Dubart-Kupperschmitt A, *et al*: Caspase-8 prevents sustained activation of NF-kappaB in monocytes undergoing macrophagic differentiation. Blood 109: 1442-1450, 2007.
62. Muendlein HI, Jetton D, Connolly WM, Eidell KP, Magri Z, Smirnova I and Poltorak A: cFLIPL protects macrophages from LPS-induced pyroptosis via inhibition of complex II formation. Science 367: 1379-1384, 2020.

Copyright © 2024 Liu et al. This work is licensed under a Creative Commons Attribution-NonCommercial-NoDerivatives 4.0 International (CC BY-NC-ND 4.0) License.